

Structural Requirements and Reaction Pathways in Dimethyl Ether Combustion Catalyzed by Supported Pt Clusters

Akio Ishikawa,[†] Matthew Neurock,^{*,‡} and Enrique Iglesia^{*,†}

Contribution from the Department of Chemical Engineering, University of California, Berkeley, California 94720, and Departments of Chemical Engineering and of Chemistry, University of Virginia, Charlottesville, Virginia 22904

Received June 8, 2007; E-mail: igelesia@berkeley.edu (E.I.); mn4n@virginia.edu (M.N.)

Abstract: The identity and reversibility of the elementary steps required for catalytic combustion of dimethyl ether (DME) on Pt clusters were determined by combining isotopic and kinetic analyses with density functional theory estimates of reaction energies and activation barriers to probe the lowest energy paths. Reaction rates are limited by C–H bond activation in DME molecules adsorbed on surfaces of Pt clusters containing chemisorbed oxygen atoms at near-saturation coverages. Reaction energies and activation barriers for C–H bond activation in DME to form methoxymethyl and hydroxyl surface intermediates show that this step is more favorable than the activation of C–O bonds to form two methoxides, consistent with measured rates and kinetic isotope effects. This kinetic preference is driven by the greater stability of the CH₃OCH₂* and OH* intermediates relative to chemisorbed methoxides. Experimental activation barriers on Pt clusters agree with density functional theory (DFT)-derived barriers on oxygen-covered Pt(111). Measured DME turnover rates increased with increasing DME pressure, but decreased as the O₂ pressure increased, because vacancies (*) on Pt surfaces nearly saturated with chemisorbed oxygen are required for DME chemisorption. DFT calculations show that although these surface vacancies are required, higher oxygen coverages lead to lower C–H activation barriers, because the basicity of oxygen adatoms increases with coverage and they become more effective in hydrogen abstraction from DME. Water inhibits reaction rates via quasi-equilibrated adsorption on vacancy sites, consistent with DFT results indicating that water binds more strongly than DME on vacancies. These conclusions are consistent with the measured kinetic response of combustion rates to DME, O₂, and H₂O, with H/D kinetic isotope effects, and with the absence of isotopic scrambling in reactants containing isotopic mixtures of ¹⁸O₂–¹⁶O₂ or ¹²CH₃O¹²CH₃–¹³CH₃O¹³–CH₃. Turnover rates increased with Pt cluster size, because small clusters, with more coordinatively unsaturated surface atoms, bind oxygen atoms more strongly than larger clusters and exhibit lower steady-state vacancy concentrations and a consequently smaller number of adsorbed DME intermediates involved in kinetically relevant steps. These effects of cluster size and metal–oxygen bond energies on reactivity are ubiquitous in oxidation reactions requiring vacancies on surfaces nearly saturated with intermediates derived from O₂.

1. Introduction

Dimethyl ether (DME) can be produced via dehydration of methanol or via direct conversion of synthesis gas.^{1–3} DME is relatively inert, noncorrosive, and nontoxic² and resembles liquefied petroleum gas (LPG) in its physical properties. As a result, it has emerged as a convenient energy carrier for distributed power generation, space heating, and diesel replacement in developing economies. Recent studies have addressed steam reforming of DME on supported metal catalysts^{4–7} and

its homogeneous combustion pathways via radical intermediates.^{8,9} Here, we explore the catalytic combustion of DME because of its potential use in power generation and radiant heating devices and its ability to combust with low emissions of NO_x, CO, and organic volatile compounds.

The first study of catalytic DME combustion reported that the specific reactivity of noble metals (per exposed metal surface atom) increased in the sequence Ru > Pt > Ir > Pd > Rh,¹⁰ but such reactivity trends were measured on clusters of different dispersions [Ru (0.06), Pt (0.41), Ir (0.76), Pd (0.23), and Rh (0.46)]. As a result, the trends may reflect the ubiquitous effects of cluster size on surface reactivity, as reported for many

[†] University of California.

[‡] University of Virginia.

- (1) Li, J. -L.; Zhang, X. -G.; Inui, T. *Appl. Catal., A* **1996**, *147*, 23.
- (2) Fleisch, T. H.; Basu, A.; Gradassi, M. J.; Masin, J. G. *Stud. Surf. Sci. Catal.* **1997**, *107*, 117.
- (3) Fleisch, T. H.; Sills, R. A. *Stud. Surf. Sci. Catal.* **2004**, *147*, 31.
- (4) Galvita, V. V.; Semin, G. L.; Belyaev, V. D.; Yurieva, T. M.; Sobyenin, V. A. *Appl. Catal., A* **2001**, *216*, 85.
- (5) Takeishi, K.; Suzuki, H. *Appl. Catal., A* **2004**, *260*, 111.
- (6) Nishiguchi, T.; Oka, K.; Matsumoto, T.; Kanai, H.; Utani, K.; Imamura, S. *Appl. Catal., A* **2006**, *301*, 66.

- (7) Faungnawakij, K.; Tanaka, Y.; Shimoda, N.; Fukunaga, T.; Kawashima, S.; Kikuchi, R.; Eguchi, K. *Appl. Catal., A* **2006**, *304*, 40.
- (8) Curran, H. J.; Fisher, S. L.; Dryer, F. L. *Int. J. Chem. Kinet.* **2000**, *32*, 741.
- (9) Curran, H. J.; Pitz, W. J.; Westbrook, C. K.; Dagaut, P.; Boettner, J. -C.; Cathonnet, M. *Int. J. Chem. Kinet.* **1997**, *30*, 229.
- (10) Solymosi, F.; Cserényi, J.; Ovári, L. *Catal. Lett.* **1997**, *44*, 89.

catalytic reactions,^{11–14} instead of intrinsic reactivity differences among these metals. In methane combustion, for example, the requirement for oxygen atom and vacancy site (O*–*) pairs and the effects of cluster size on oxygen binding energy lead to marked effects of cluster size on turnover rates.^{15–18}

We provide here kinetic, isotopic, and theoretical evidence for the identity and kinetic relevance of the elementary steps involved in DME combustion on Pt clusters over a wide range of dispersions (0.26–0.99; ~1–4 nm diameter) supported on γ -Al₂O₃ and ZrO₂. These details are essential for a rigorous description of intrinsic reactivity and for the practical implementation of catalytic DME combustion within complex hydrodynamic environments that exhibit ubiquitous temperature and concentration gradients. This study provides evidence for the relevance of C–H bond activation steps in molecularly adsorbed DME and for the role of vacancies within chemisorbed oxygen layers in the catalysis of such steps. Turnover rates decreased with increasing Pt dispersion because of the concomitant increase in the coordinative unsaturation of exposed metal atoms and in the binding energy of chemisorbed oxygen atoms with decreasing cluster size, which led in turn to a smaller number of vacancies on nearly saturated surfaces.

2. Experimental Methods

2.1. Catalyst Synthesis and Characterization. γ -Al₂O₃ (193 m² g⁻¹) was prepared by treating Al₂O₃ (Sasol North America Inc., lot no. C1643) in flowing dry air (Praxair, 99.99%, 0.8 cm³ g⁻¹ s⁻¹) at 923 K (0.083 K s⁻¹) for 5 h. ZrO₂ (monoclinic, 34 m² g⁻¹) was prepared as described previously.^{19,20} ZrO₂ precursors obtained by precipitation of ZrOCl₂·8H₂O (Aldrich, CAS no. 13520-92-8) were treated in flowing dry air at 1023 K for 5 h and at 923 K for 5 h. The crystal structure and surface area of the supports were characterized by X-ray diffraction (XRD; Siemens, D 500, Cu K α radiation) and N₂ adsorption at 77 K using an Autosorb 6 system (Quantachrome, Inc), respectively.

Supported Pt catalysts were prepared by incipient wetness impregnation of γ -Al₂O₃ and ZrO₂ with aqueous H₂PtCl₆·6H₂O solutions (Aldrich, CAS no. 16941-12-1). Impregnated samples were treated in ambient air at 393 K and then in flowing dry air (0.7 cm³ g⁻¹ s⁻¹) at 823 K (0.083 K s⁻¹) for 5 h. The samples were then treated in pure H₂ (Praxair, 99.999%, 0.8 cm³ g⁻¹ s⁻¹) at 723 K (0.083 K s⁻¹) for 2 h and in 1% O₂/He (Praxair, 0.4 cm³ g⁻¹ s⁻¹) at ambient temperature for 1 h to passivate them before exposure to ambient air and use in rate and chemisorption measurements. Pt contents were measured by ICP-OES (Galbraith Laboratories). Pt/Al₂O₃ (0.8, 0.9, and 2.3 wt %) and Pt/ZrO₂ (1.0 and 1.1 wt %) samples were prepared as shown in Table 1. Portions of 0.9 wt % Pt/Al₂O₃ and 1.0 wt % Pt/ZrO₂ samples were then treated again in (i) flowing dry air (0.7 cm³ g⁻¹ s⁻¹) at different temperatures (823–923 K) and then in H₂ at 723 K for 2 h or (ii) flowing H₂ at temperatures above 723 K (773–923 K) to vary their metal dispersion; these samples were also passivated in 1% O₂/He before exposure to ambient air and subsequent use for chemisorption and catalytic measurements.

Pt dispersions were measured from volumetric uptakes of strongly chemisorbed H₂ at 313 K using a Quantasorb chemisorption analyzer

Table 1. Pt Dispersions, Average Crystallite Diameters, and DME Combustion Turnover Rates (Extrapolated to Zero Residence Time and Conversion)^a

catalyst	Pt dispersion	crystallite diam ^b (nm)	DME turnover rate ^c
0.8 wt % Pt/Al ₂ O ₃	0.99	1.2	0.11
0.9 wt % Pt/Al ₂ O ₃	0.75	1.6	0.20
2.3 wt % Pt/Al ₂ O ₃	0.50	2.3	0.40
0.9 wt % Pt/Al ₂ O ₃	0.52	2.2	0.33
1.1 wt % Pt/ZrO ₂	0.44	2.5	0.35
1.0 wt % Pt/ZrO ₂	0.42	2.7	0.55
1.0 wt % Pt/ZrO ₂	0.36	3.2	0.63
1.0 wt % Pt/ZrO ₂	0.26	4.4	1.18

^a Conditions: 473 K, 2 kPa of DME, 20 kPa of O₂, balance He.

^b Estimated from fractional Pt dispersion assuming hemispherical clusters.

^c Units of mol of DME/(mol of surface Pt s).

(Quantachrome Corp.). H₂ adsorption isotherms were measured at 3–50 kPa of H₂ after passivated samples were treated in pure H₂ at 673 K for 1 h and then in a dynamic vacuum at 673 K for 1 h. A back-sorption isotherm was then measured after evacuation at 313 K for 0.5 h to determine uptakes of weakly bound hydrogen. Pt dispersions were measured from the difference between these two isotherms extrapolated to zero H₂ pressure by assuming a 1:1 H:Pt adsorption stoichiometry. Average cluster diameters were estimated from these dispersion values by assuming hemispherical clusters and using the density of bulk Pt metal²¹ (21.45 g cm⁻³). Dispersions and cluster sizes are reported in Table 1. X-ray absorption near-edge spectroscopy (XANES) did not detect bulk oxidation of Pt clusters during DME combustion catalysis at 473 K (Supporting Information); Pt clusters are therefore denoted as Pt metal.

2.2. Steady-State Catalytic DME Combustion Reactions. Catalytic rates were measured on catalysts (5 mg, 250–425 μ m particle size) diluted within pellets with inert supports (SiO₂, 280 m² g⁻¹, Chromatographic Silica Media, CAS no. 112926-00-8) to avoid temperature and concentration gradients and to ensure strict kinetic control. The catalysts (50–100 mg) diluted with SiO₂ (2.5–3.8 g) at dilution ratios of SiO₂:catalyst = 25:1, 50:1, and 75:1 were pressed at ~10 MPa and sieved to retain 106–250 or 250–425 μ m particles, and then a portion (catalyst content 5 mg) of the sieved sample was placed within a quartz tube (8 mm i.d.). The SiO₂ diluent was washed with 3 M nitric acid (EMD Chemicals Inc., CAS no. 7697-37-2, ACS reagent) and treated in dry air at 923 K for 5 h before use. Temperatures were measured with a type K thermocouple enclosed within a sheath in contact with the catalyst bed. Temperatures were within ± 0.5 K of the average bed temperature at all bed positions.

Reactant mixtures consisted of premixed gases containing 2% DME and 20% O₂ with He as the diluent (Praxair certified mixture) or of separate streams consisting of 15% DME in He (Praxair certified mixture), 90% O₂ in N₂ (Praxair certified mixture), and pure He (99.999%, Praxair), which were mixed by independent control of their respective flow rates. The effects of CO₂ and H₂O products on DME combustion rates were measured by introducing 50% CO₂/Ar (Matheson certified mixture) or by vaporizing liquid H₂O (doubly distilled, deionized water; syringe pump, Cole Parmer, 60061 series) into flowing DME–O₂ reactant streams. Heated lines (373–423 K) were used to transfer all streams into the reactor and into an Agilent 6890 gas chromatograph equipped with a methyl silicone capillary column (HP-1, 25 m \times 0.32 mm \times 1.05 μ m) connected to a flame ionization detector and a Porapak Q packed column (80–100 mesh, 12 ft \times 1/8 in.) connected to a thermal conductivity detector.

2.3. Isotopic Exchange Rates and Kinetic Isotopic Effects. Kinetic isotope effects (CH₃OCH₃–CD₃OCD₃) and isotopic exchange rates (¹²-CH₃O¹²CH₃–¹³CH₃O¹³CH₃ or ¹⁶O₂–¹⁸O₂) were measured on a 1.0 wt

(11) Valeden, M.; Lai, X.; Goodman, D. W. *Science* **1998**, *281*, 1647.

(12) Haruta, M. *Catal. Today* **1997**, *36*, 153.

(13) Markovic, N.; Gasteiger, H.; Ross, P.N. *J. Electrochem. Soc.* **1997**, *144*, 1591.

(14) Saib, A. M.; Claeys, M.; Van Steen, E. *Catal. Today* **2002**, *71*, 395.

(15) Bethke, K. A.; Kung, H. H. *J. Catal.* **1997**, *172*, 93.

(16) Wei, J.; Iglesia, E. *J. Phys. Chem. B* **2004**, *108*, 4094.

(17) Hicks, R. F.; Young, M. L.; Lee, R. G. *J. Catal.* **1990**, *122*, 295.

(18) Fujimoto, K.; Ribeiro, F. H.; Avalos-Borja, M.; Iglesia, E. *J. Catal.* **1998**, *179*, 431.

(19) Wei, J.; Iglesia, E. *J. Phys. Chem. B* **2004**, *108*, 7253.

(20) Barton, D. G. Ph.D. Dissertation, University of California at Berkeley, 1998.

(21) David, R. L. *Handbook of Chemistry and Physics*, 87th ed.; CRC Press: Boca Raton, FL, 2006.

% Pt/ZrO₂ (0.42 dispersion) catalyst using a gradientless recirculating batch reactor. Reactants and products were circulated at 1.7 cm³ s⁻¹ over catalyst samples (1–15 mg, diluted with SiO₂ 1:50) using a graphite gear micropump. Chemical and isotopic compositions were measured by direct sampling into a gas chromatograph equipped with mass-selective and flame ionization detectors (Agilent 6890 GC–MS system). Catalyst samples were treated in H₂ (Praxair, 99.999%, 0.7 cm³ g⁻¹ s⁻¹) at 673 K for 1 h before all measurements.

CH₃OCH₃ (Matheson, 99.5%), CD₃OCD₃ (Isotec, chemical purity >99.0%), ¹³CH₃O¹³CH₃ (Isotec, chemical purity >99.0%), 50% ¹⁶O₂/Ar (Praxair, 99.99%), ¹⁶O₂ (Praxair, 99.99%), ¹⁸O₂ (Isotec, chemical purity >99 atom % ¹⁸O), and He (Praxair, balance to give a 110 kPa total pressure) were used as reagents, and Ar (3 kPa) was introduced as an internal standard. Trace impurities (<1.0%) in CD₃OCD₃ and ¹³CH₃O¹³CH₃ led to catalyst deactivation and required further purification of these reactants by trapping impurities at 77–273 K.

2.4. Computational Methods. Ab initio density functional theory (DFT) quantum chemical calculations were carried out to determine adsorption and reaction energies and activation barriers for various elementary steps using periodic plane wave density functional theory as implemented in the Vienna Ab Initio Simulation Program (VASP).^{22–24} The PW91 functional form of the generalized gradient approximation was used to calculate nonlocal corrections to the exchange and correlation energies.²⁵ The electron–ion interactions were described using ultrasoft pseudopotentials²⁶ with a plane wave cutoff energy of 396.0 eV. A 3 × 3 × 1 Monkhorst–Pack *k*-point mesh²⁷ was used to sample the first Brillouin zone. The Pt surface was treated as an ideal Pt(111) substrate comprised of four metal layers separated by 15 Å of vacuum. The bottom two layers of the slab were held fixed at their bulk lattice positions while the top two layers were allowed to relax. A 3 × 3 unit cell consisting of 9 metal atoms per layer (36 total Pt atoms) was used to simulate the adsorption of DME and its initial reaction paths over Pt(111) surfaces with different coverages of chemisorbed oxygen. The structures as well as the first two layers of the Pt surface were optimized such that the total free energies and the band structure energies converged to within 1 × 10⁻⁴ eV. Subsequent calculations were carried out on three metal layer substrates and 2 × 2 unit cells to test the level of accuracy of the energy estimates. Reaction energies varied by less than 3 kJ mol⁻¹, indicating that the calculations reported on the larger system provide an acceptable level of accuracy. The activation barriers were all determined using the nudged elastic band climbing (NEB-CI) method developed by Jonsson²⁸ and described in detail elsewhere.²⁹

3. Results and Discussion

3.1. DME Catalytic Oxidation on Supported Pt Metal Clusters at Low Temperature (423–523 K). The catalytic combustion of DME on Pt-based catalysts forms only CO₂ and H₂O. Figure 1 shows DME conversion with and without catalyst (1.0 wt % Pt/ZrO₂, 0.26 dispersion) as a function of reaction temperature (2 kPa of DME, 20 kPa of O₂, He balance). DME combustion products (CO₂, H₂O) became detectable at ~423 K on Pt/ZrO₂. Figure 1 also shows CO₂ formation rates from

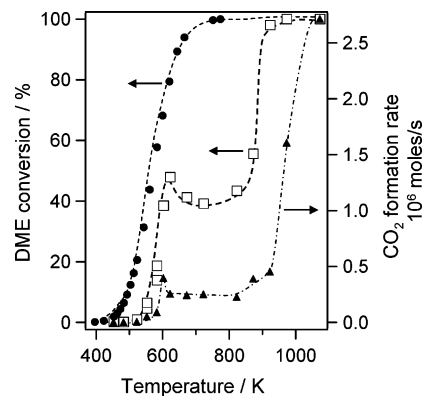
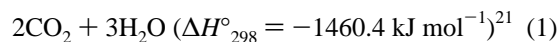
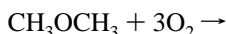


Figure 1. DME conversion as a function of temperature during (●) catalysis on 1.0 wt % Pt/ZrO₂ (5 mg, 0.26 dispersion) and (□) gas-phase reaction (without a catalyst) and (▲) CO₂ formation rate as a function of temperature for gas-phase reaction [2 kPa of DME, 20 kPa of O₂, balance He, DME inlet molar flow rate 1.37 × 10⁻⁶ mol s⁻¹].

homogeneous DME combustion pathways. These homogeneous DME oxidation and pyrolysis radical chain reactions become detectable only above 523 K and predominantly formed CO, CO₂, CH₄, HCHO, HCOOH, and H₂O.^{8,30} Homogeneous DME pyrolysis and oxidation rates initially increased, then decreased, and ultimately again increased with increasing temperature, as also previously reported;⁸ these trends reflect changes in the concentration of reactive OH radicals with increasing temperature. Homogeneous pathways formed HCHO, CO₂, CH₃OH, and HCOOH below 973 K in our experiments; CO₂ and H₂O became the only products above 1073 K. Homogeneous combustion reactions required much higher temperatures than catalytic combustion on Pt-based catalysts and led to negligible contributions to the catalytic rates reported here at 423–523 K.

Turnover rates for highly exothermic reactions, such as DME combustion



must be measured under strict kinetic control without ubiquitous transport artifacts that lead to temperature and concentration gradients within pellets or packed beds. These artifacts can be detected and removed only by intrapellet and bed dilution of catalysts with inert solids. Figure 2 shows DME combustion turnover rates as a function of residence time at 473 K on 1.0 wt % Pt/ZrO₂ (0.26 dispersion) for different pellet diameters and extents of dilution. At low dilution levels (25:1), local temperatures exceed those measured and rates become artificially high as a result of these artifacts. Higher dilution ratios eliminated these artifacts and led to reaction rates that did not depend on pellet diameters (105–250 vs 250–425 μm) or on additional intrapellet dilution (50:1 vs 75:1) (Figure 2). DME combustion turnover rates decreased with increasing residence time because of the combined effects of reactant depletion (3–14% DME conversion) and inhibition by products, as discussed below. All rates reported henceforth were measured at the highest dilution level and extrapolated to zero reactant residence times, except for those measured with H₂O and CO₂ added to reactants, which are reported at the prevailing DME conversion levels.

- (22) Kresse, G.; Hafner, J. *Phys. Rev. B* **1993**, *47*, 558.
 (23) Kresse, G.; Furthmüller, J. *Comput. Mater. Sci.* **1996**, *6*, 15.
 (24) Kresse, G.; Furthmüller, J. *Phys. Rev. B* **1996**, *54*, 11169.
 (25) Perdew, P.; Chevary, J. A.; Vosko, S. H.; Jackson, K. A.; Pederson, M. R.; Singh, D. J.; Fiolhais, C. *Phys. Rev. B* **1992**, *46*, 6671.
 (26) Vanderbilt, D. *Phys. Rev. B* **1990**, *41*, 7892.
 (27) Monkhorst, H. J.; Pack, J. D. *Phys. Rev. B* **1976**, *13*, 5188.
 (28) Henkelman, G.; Uberuaga, B. P.; Jonsson, H. *J. Chem. Phys.* **2000**, *113*, 9901.
 (29) The nudged elastic band is first used to optimize the forces along a set of fixed points chosen here to be equally spaced along the reaction path between the reactant and product. The climbing algorithm is subsequently used to isolate the point of highest energy. This method increases the energy of the structures along the reaction path to more quickly converge upon the transition state.

- (30) Rosado-Reyes, C. M.; Francisco, J. S.; Szenté, J. J.; Maricq, M. M.; Østergaard, L. F. *J. Phys. Chem. A* **2005**, *109*, 10940.

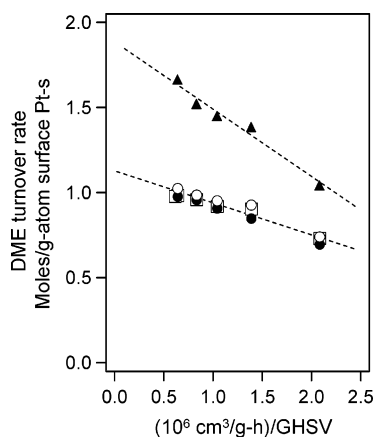


Figure 2. DME combustion turnover rates as a function of residence time on 1.0 wt % Pt/ZrO₂ (5 mg, 0.26 dispersion) at 473 K for various pellet diameters and SiO₂:catalyst intrapellet dilution ratios: (▲) 250–450 μm, 25:1; (●) 250–450 μm, 50:1; (□) 250–450 μm, 75:1; (○) 106–250 μm, 50:1 (2 kPa of DME, 20 kPa of O₂, balance He).

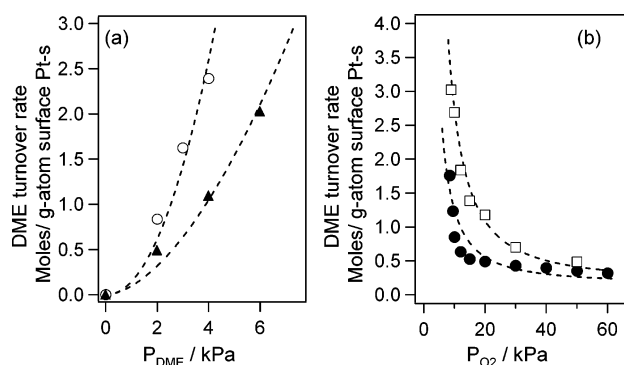


Figure 3. Effects of DME (a) and O₂ (b) partial pressures on DME combustion turnover rates on 1.0 wt % Pt/ZrO₂ (5 mg, 0.42 dispersion, 250–450 μm, 50:1) at 473 K [(○) 10 kPa and (▲) 20 kPa of O₂ in (a) and (●) 2 kPa and (□) 4 kPa of DME in (b)].

3.2. Kinetic Dependence of Dimethyl Ether Combustion Rate on Reactant Partial Pressures. The kinetic response of DME combustion rates to DME and O₂ partial pressures was measured on Pt/ZrO₂ (1.0 wt %, 0.42 dispersion) catalysts at 473 K. Figure 3a shows the effects of DME pressure on combustion turnover rates at two different O₂ pressures (10 and 20 kPa). DME turnover rates increased faster than linearly with increasing DME pressure. The effects of O₂ on DME combustion turnover rates are shown in Figure 3b at two different DME pressures (2 and 4 kPa). At both DME pressures (2 and 4 kPa), combustion rates on Pt catalysts decreased with increasing O₂ pressure at low O₂ pressures (<20 kPa), but became nearly independent of O₂ pressure as O₂ pressures increased.

Adsorption of O₂ on reduced Pt clusters (Pt/Al₂O₃) leads to a nearly saturated monolayer of chemisorbed oxygen at 300 K.³¹ The high activation energy for recombinative desorption of oxygen from nearly saturated Pt surfaces [$\sim 175 \pm 10$ kJ mol⁻¹ on 2.9 wt % Pt/Al₂O₃ (0.85 dispersion);³¹ Pt(110),³² $\sim 199 \pm 10$ kJ mol⁻¹] prevents equilibration of dissociative chemisorption steps at temperatures below ~ 800 K. Reductants such as CO and H₂, however, can remove chemisorbed oxygen atoms from Pt surfaces at nearly ambient temperatures.³³ The kinetic

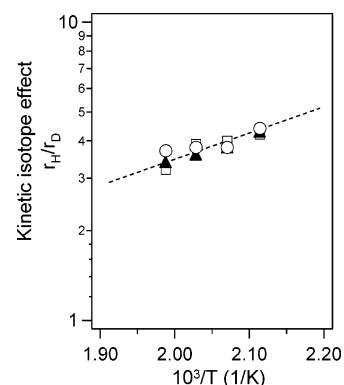


Figure 4. Kinetic isotope effects for DME combustion on 1.0 wt % Pt/ZrO₂ catalysts (5–10 mg, 0.42 dispersion, 250–450 μm, 50:1) at various temperatures and reactant pressures [(□) 10 kPa, (▲) 20 kPa, and (○) 50 kPa of O₂ and 2 kPa of CH₃OCH₃ or CD₃OCD₃].

response of DME turnover rates to DME and O₂ pressures may reflect the requirement for vacancy sites (*) on oxygen-covered Pt surfaces for DME activation and also the role of DME as the reductant required to form such sites within catalytic redox cycles. Fujimoto et al.¹⁸ proposed that CH₄ combustion pathways on PdO_x crystallites involve the activation of CH₄ on site pairs consisting of oxygen atoms (O*) and oxygen vacancies (*). The availability of such O*–* site pairs depends on reactant and product (H₂O, CO₂) pressures and on the size of active PdO_x clusters. The effect of DME and O₂ partial pressures on the surface concentration of O*–* site pairs leads to the measured dependence of turnover rates on DME and O₂ partial pressures, as we discuss below. DME and O₂ kinetic orders of 2.0 ± 0.2 and -1.0 ± 0.3 , respectively, were measured by regression (dashed curves) of the data in Figure 3 to a simple power law model. The dashed curves in Figure 3 show that DME turnover rates can be accurately described by a rate equation of the form

$$r = k[\text{DME}]^2[\text{O}_2]^{-1} \quad (2)$$

3.3. CH₃OCH₃–CD₃OCD₃ Kinetic Isotope Effects. Kinetic isotope effects ($r_{\text{H}}/r_{\text{D}}$) were measured from DME combustion rates (extrapolated to zero conversion) using CH₃OCH₃–O₂ or CD₃OCD₃–O₂ reactants (2 kPa of DME) at several temperatures (473, 483, 493, and 503 K) and O₂ partial pressures (10, 20, and 50 kPa) using a recirculating gradientless batch reactor. Measured kinetic isotope effects (KIEs) are shown in Figure 4. These KIE values are significantly larger than unity, indicating that the kinetically relevant steps involve the activation of C–H bonds, and not C–O bonds, in DME-derived intermediates. These KIE values did not depend on O₂ pressures, indicating that the relative importance of any denominator terms in the more complex equations derived below did not vary with O₂ pressure. Similar KIE values were reported previously for C–H bond activation in methoxide species (CH₃O*) involved in kinetically relevant steps during methanol oxidation on MoO₃-supported (533 K, KIE = 4.2) and RuO_x/TiO₂ (393 K, KIE = 2.5) catalysts.^{34–36} DME oxidation to formaldehyde on MoO₃/Al₂O₃ catalysts also involves methoxide species formed via dissociative adsorption of DME,³⁷ but C–O bond cleavage

(31) Bourne, A.; Bianchi, D. *J. Catal.* **2002**, *209*, 114.

(32) Wartnaby, C. E.; Stuck, A.; Yeo, Y. Y.; King, D. A. *J. Chem. Phys.* **1995**, *102*, 1855.

(33) Bourne, A.; Bianchi, D. *J. Catal.* **2004**, *220*, 4.

(34) Holstein, W. L.; Machiels, C. J. *J. Catal.* **1996**, *162*, 118.

(35) Machiels, C. J.; Sleight, A. W. *J. Catal.* **1982**, *76*, 238.

(36) Liu, H.; Iglesia, E. *J. Phys. Chem. B* **2005**, *109*, 2155.

(37) Cheung, P.; Liu, H.; Iglesia, E. *J. Phys. Chem. B* **2004**, *108*, 18650.

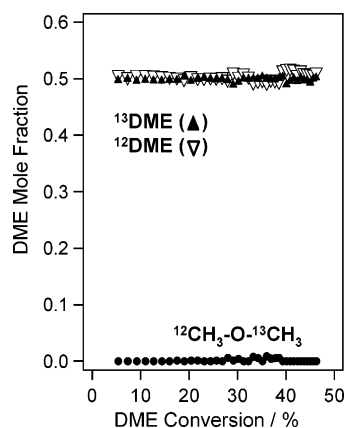


Figure 5. $^{12}\text{CH}_3\text{O}^{13}\text{CH}_3$ mole fractions in CH_3OCH_3 reactants during reactions of $^{12}\text{CH}_3\text{O}^{12}\text{CH}_3$ – $^{13}\text{CH}_3\text{O}^{13}\text{CH}_3$ and O_2 on 1.0 wt % Pt/ZrO₂ (5 mg, 0.42 dispersion, 250–450 μm , 50:1) at 473 K [1 kPa of $^{12}\text{CH}_3\text{O}^{12}\text{CH}_3$, 1 kPa of $^{13}\text{CH}_3\text{O}^{13}\text{CH}_3$, 20 kPa of O_2 , 3 kPa of Ar, balance He].

leading to methoxide formation is the kinetically relevant step, and this reaction shows very weak kinetic isotope effects. Thus, it seems plausible at first to attribute the measured KIE values for DME oxidation to the relative rates of hydrogen abstraction from CH_3O^* and CD_3O^* surface species. It is also possible that these isotope effects reflect the kinetically relevant activation of C–H bonds in molecularly adsorbed DME, as proposed from vibrational spectra and desorption dynamics on Rh surfaces at subambient temperatures (250–300 K)³⁸ and also suggested by the difficult C–O bond activation in DME oxidation to formaldehyde on MoO_x-based catalysts.³⁷ These two possible pathways cannot be discerned from these data because they can lead to similar rate equations; thus, we require a more rigorous analysis of the elementary steps involved in DME activation and of the isotopic exchange data that we present below.

3.4. Isotopic Evidence for the Irreversible Character of DME and O₂ Dissociation Steps. Reactions of $^{12}\text{CH}_3\text{O}^{12}\text{CH}_3$ – $^{13}\text{CH}_3\text{O}^{13}\text{CH}_3$ – O_2 mixtures were used to probe the rates of recombinative desorption of DME-derived methoxide intermediates. Figure 5 shows the distribution of DME isotopomers during DME combustion on Pt/ZrO₂ (1.0 wt %, 0.42 dispersion) at 473 K in the recirculating batch reactor. Mixed $^{12}\text{CH}_3\text{O}^{13}\text{CH}_3$ isotopomers were not detected at any DME chemical conversion level (0–50%), indicating that the formation of methoxide species via C–O cleavage in molecularly adsorbed DME is irreversible or that the C–O bond cleavage ultimately required for the formation of CO and CO₂ in DME combustion reactions on Pt occurs only after all kinetically relevant steps.

The reversibility of dissociative O₂ chemisorption steps was probed by measuring $^{16}\text{O}^{18}\text{O}$ formation rates during reactions of $\text{CH}_3^{16}\text{OCH}_3$ with equimolar $^{16}\text{O}_2$ – $^{18}\text{O}_2$ mixtures (2 kPa of DME, 10 kPa of $^{16}\text{O}_2$, 10 kPa of $^{18}\text{O}_2$). Quasi-equilibrated dissociation steps would lead to binomial isotopomer distributions (50% $^{16}\text{O}^{18}\text{O}$). Mixed isotopomers were not detected at 473 or 503 K over a wide range of DME chemical conversions (0–50%, Figure 6). These data show that O₂ dissociation steps are irreversible; $^{16}\text{O}^{18}\text{O}$ detection limits indicate that recombinative desorption rates are >200 times lower than DME chemical conversion rates at 473 K. These conclusions are consistent with the strong binding of chemisorbed oxygen on Pt surfaces³⁹ and with the high activation energies for recom-

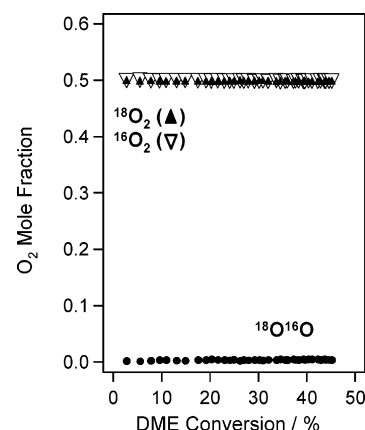
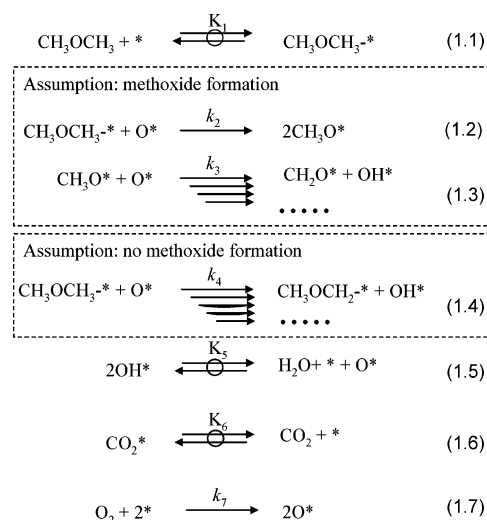


Figure 6. $^{16}\text{O}^{18}\text{O}$ mole fractions in O_2 reactants during reactions of $\text{CH}_3^{16}\text{OCH}_3$ and equimolar $^{16}\text{O}_2$ – $^{18}\text{O}_2$ on 1.0 wt % Pt/ZrO₂ (5 mg, 0.42 dispersion, 250–450 μm , 50:1) at 473 K [2 kPa of DME, 10 kPa of $^{16}\text{O}_2$, 10 kPa of $^{18}\text{O}_2$, 3 kPa of Ar, balance He].

Scheme 1. Reaction Pathways for the Oxidation of DME on Supported Pt Clusters, Including the Alternate Assumptions of (i) Methoxide Formation via DME Dissociative Adsorption and (ii) No Methoxide Formation



binative desorption of O₂ on Pt single-crystal surfaces ($\sim 199 \pm 10 \text{ kJ mol}^{-1}$),³⁰ which would preclude adsorption–desorption equilibration at 423–523 K.

3.5. Plausible Elementary Steps Involved in Dimethyl Ether Activation and Combustion. The lack of methyl exchange between labeled and unlabeled DME (section 3.4) indicates that methoxide formation via DME dissociation is either irreversible or kinetically irrelevant. We consider next the kinetic implications of (1) an irreversible DME dissociation step followed by H-abstraction and (2) an alternate route via H-abstraction from undissociated molecular DME and consider these steps as kinetically relevant. We examine here the sequence of elementary steps shown in Scheme 1, which includes these two routes for C–H bond activation: (i) C–H activation from methoxide species formed after irreversible DME dissociation (steps 1.2 and 1.3) and (ii) C–H activation in molecularly adsorbed DME (step 1.4). In both routes, surface vacancies (*) form via quasi-equilibrated recombination of two hydroxyl species (OH*) to give water (step 1.5) and the

(38) Bugyi, L.; Solymosi, F. *Surf. Sci.* **1997**, *385*, 365.

(39) van Santen, R. A.; Neurock, M. *Molecular Heterogeneous Catalysis*; Wiley-VCH Verlag GmbH & Co. KgaA: Weinheim, Germany, 2006.

$$r = \frac{2k_7[\text{O}_2]}{4.5 \times \left[1 + \frac{k_7[\text{O}_2]}{4.5 K_1 k_2 [\text{CH}_3\text{OCH}_3]} + K_1 [\text{CH}_3\text{OCH}_3] + \frac{2K_1 k_2 [\text{CH}_3\text{OCH}_3]}{k_3} + \frac{k_7 [\text{H}_2\text{O}][\text{O}_2]}{4.5 K_1 K_3 k_2 [\text{CH}_3\text{OCH}_3]} + \frac{[\text{CO}_2]}{K_6} \right]^2} \quad (3)$$

\vdots
 $*$ O^* DME^* CH_3O^* OH^* CO_2^*

$$r = \frac{k_7[\text{O}_2]}{4.5 \times \left[1 + \frac{k_7[\text{O}_2]}{4.5 K_1 k_4 [\text{CH}_3\text{OCH}_3]} + K_1 [\text{CH}_3\text{OCH}_3] + \frac{k_7 [\text{H}_2\text{O}][\text{O}_2]}{4.5 K_1 K_3 k_4 [\text{CH}_3\text{OCH}_3]} + \frac{[\text{CO}_2]}{K_6} \right]^2} \quad (4)$$

\vdots
 $*$ O^* DME^* OH^* CO_2^*

sequence is completed via a set of kinetically irrelevant steps that ultimately lead to the desorption of CO_2 (step 1.6). DME adsorbs on surface vacancies (*) in a quasi-equilibrated adsorption–desorption step (step 1.1). This is supported by DFT calculations reported below in section 3.6 which show that the bond between DME and the Pt(111) surface is rather weak. Surface O^* species are replenished via irreversible dissociative chemisorption of O_2 coreactants (step 1.7). These two derivations and the measured KIE values (4.2–3.2 at 473–503 K) indicate that hydrogen abstractions from methoxide species (step 1.3, k_3) and from molecularly adsorbed DME (step 1.4, k_4) are the respective kinetically relevant steps in these two possible catalytic sequences. If the respective rate equations derived from the sequence of elementary steps do not contain k_3 or k_4 parameters, those steps become kinetically irrelevant; as a result, rate equations without k_3 or k_4 and the mechanisms giving rise to such rate equations are inconsistent with the measured KIE values.

Pseudo-steady-state concentrations for all adsorbed species in Scheme 1 lead to complex kinetic rate expressions for the cases of (i) C–H abstraction from methoxide species (eq 3) and (ii) C–H activation from molecularly adsorbed DME (eq 4). Their full algebraic derivations are included in Appendices 1 and 2 in the Supporting Information, and only the final equations are listed here.

Each term in the denominator of these equations represents the concentration of the indicated adsorbed intermediate, relative to the concentration of vacancy sites. Equations 3 and 4 become eqs 5 and 6,

$$r = \frac{9K_1^2 k_2^2 [\text{DME}]^2}{k_7 [\text{O}_2]} \quad (5)$$

$$r = \frac{4.5K_1^2 k_4^2 [\text{DME}]^2}{k_7 [\text{O}_2]} \quad (6)$$

respectively, when O^* species are the most abundant surface intermediates (MASIs). Both rate equations are consistent with the kinetic data in Figure 3 (eq 2); we have found no other sequence of elementary steps or combinations of steady-state and MASI assumptions consistent with these measured kinetic data.

Equation 5, corresponding to activation of methoxide species formed via DME dissociation, however, predicts very weak H–D isotope effects arising from equilibrated DME molecular

adsorption (step 1.1, K_1) and irreversible DME dissociation (step 1.2, k_2), but lacks any kinetic or thermodynamic parameters for elementary steps involving C–H bond activation (step 1.3, k_3). Thus, the sequence involving C–H activation of chemisorbed methoxide intermediates (steps 1.2 and 1.3) cannot be responsible for DME combustion on Pt cluster surfaces. In contrast, eq 6 includes the rate constant for H-abstraction from molecularly adsorbed DME (k_4). It is, therefore, consistent with measured KIE values (4.2–3.2 at 473–503 K). Equation 6 indicates that KIE values for DME combustion depend on the ratio of rate constants given by

$$\text{KIE} = \frac{(K_{1,\text{H}} k_{4,\text{H}})^2 k_{7,\text{D}}}{(K_{1,\text{D}} k_{4,\text{D}})^2 k_{7,\text{H}}} \quad (7)$$

H-abstraction (step 1.4, k_4) from adsorbed DME is expected to show a normal H–D kinetic isotope effect, while equilibrated DME adsorption (step 1.1, K_1) and reoxidation of the vacancy sites (step 1.7, k_7) would give small or no isotope effects, respectively. We note also that the constant KIE values measured as a function of O_2 are consistent with the presence of a single dominant term in the denominator of eq 4, as indicated by its simplified form given by eq 6 used to describe the data in Figure 3.

Figure 7 shows parity plots for measured DME turnover rates (Figure 3) and those calculated from eq 6. The kinetic parameters derived from this regression analysis are reported in Table 2. Turnover rates calculated from this kinetic expression agree with measured rates. A comparison of methanol and DME combustion rates, discussed next, confirms that DME dissociation and the subsequent activation of C–H bonds in the methoxide species formed are not responsible for measured DME combustion rates on Pt cluster surfaces.

If the methoxide intermediates shown to mediate methanol oxidation catalysis were also kinetically relevant in DME oxidation, the rates of these two reactions would be similar as these methoxide species become the MASIs. Methanol and DME oxidation rates on Pt/ZrO₂ (1.0 wt %, 0.42 dispersion) are shown in Figure 8 as CO_2 formation rates. Methanol oxidation formed formaldehyde, methyl formate (MF), and CO_2 and H_2O at lower temperatures (313–423 K) than DME combustion to form CO_2 and H_2O (473–523 K). These methanol oxidation rates are similar to those reported previously on Pt-based catalysts.^{40–42} MF forms via HCHO reactions with methoxide intermediates.³⁶ We note that (i) methanol oxidation

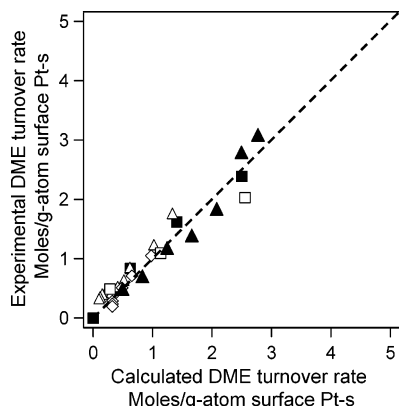


Figure 7. Parity plots for the calculated DME turnover rates using kinetic rate expression (eqs 6 and 10) and DME turnover rates as shown in Figures 3 and 14 [DME effects (Figure 3a), (■) 10 kPa of O₂, (□) 20 kPa of O₂; O₂ effects (Figure 3b), (△) 2 kPa of DME, (▲) 4 kPa of DME; H₂O effects (Figure 14), (◇) 5 kPa of H₂O].

Table 2. Parameters for the Kinetic Model for Figure 7

rate expression	$(K_1 k_4)^2 / k_7$ [mol/(mol of surface Pt s kPa)]	$K_1 k_4 K_5$ (mol/(mol of surface Pt s))
$r^a = 4.5 K_1^2 k_4^2 [\text{DME}]^2 / k_7 [\text{O}_2]$	0.35 ± 0.012	
$r^b = K_1 k_4 K_5 [\text{DME}] / [\text{H}_2\text{O}]$		0.82 ± 0.042

^a DME turnover rates without addition of H₂O, eq 6. ^b DME turnover rates with addition of H₂O, eq 10.

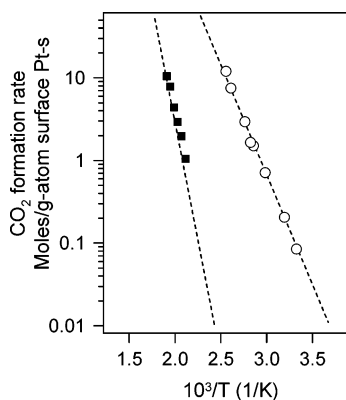


Figure 8. Arrhenius plot for DME (■) and methanol (○) combustion on 1.0 wt % Pt/ZrO₂ (5 mg, 0.42 dispersion, 250–450 μm, 50:1) [2 kPa of DME or 2 kPa of methanol, 20 kPa of O₂, balance He].

occurs at nearly ambient temperatures (vs ~423 K for DME combustion in Figure 1), (ii) CO₂ formation rates from methanol are much faster than CO₂ formation rates from DME on Pt/ZrO₂ catalysts (Figure 8), (iii) all methoxide intermediates formed during CH₃OH combustion reactions are converted to CO₂ at ~413 K (data not shown), and (iv) DME combustion did not form HCHO or MF products. Specifically, the C–H activation of the methoxide intermediates and CH₃OH complete oxidation to CO₂ and H₂O occur above 413 K. The kinetically relevant step is therefore much slower in the DME combustion reactions, apparently because the activation of C–O bonds to form methoxides is unfavorable and methoxides do not form before the activation of terminal C–H bonds in adsorbed DME.

Table 3. DFT-Calculated Adsorption of DME and Reactive Intermediates Bound to Pt(111)

adsorbate	oxygen coverage (ML)	binding energy (kJ mol ⁻¹)	adsorbate	oxygen coverage (ML)	binding energy (kJ mol ⁻¹)
DME (CH ₃ OCH ₃)	0	-21.0	CH ₃ OCH ₂	0	-182.4
	1/9	-19.9		1/9	
	4/9	-12.3		4/9	-107.8
	2/3	-11.0		2/3	-103.1
methoxy (CH ₃ O)	0	-144.6	oxygen (O)	1/3	-365.3
	1/9	-108.5	hydroxyl (OH)	0	-221.2
	4/9		1/9		
	2/3	-77.4	4/9	-189.1	
			2/3	-179.0	

These results, as well as the absence of HCHO and MF products during DME oxidation, indicate that DME activation on supported Pt clusters does not involve methoxide intermediates. The activation of terminal C–H bonds in DME controls reaction rates, consistent with DFT calculations described next.

3.6. Ab Initio Calculations of DME Combustion Elementary Steps on Pt(111) Surfaces at Various Oxygen Coverages. The initial C–H and C–O bond activation steps involved in DME oxidation were examined by carrying out ab initio density functional theoretical calculations on idealized Pt(111) surfaces. While the (111) surface is an incomplete representation of the active surfaces on Pt clusters, it provides a convenient starting point for a systematic assessment of the energetics that control the elementary processes of adsorption and desorption and the surface reactivity for the specific activation paths that govern reaction selectivities. The data reported below (section 3.9) also show that larger Pt clusters are much more active than smaller clusters, making the closest packed (111) surface the most relevant model for comparisons among alternate elementary steps. DFT calculations are used herein to determine the reaction energies and activation barriers for both the C–O and C–H activation paths (paths 2 and 4, respectively, in Scheme 1) involved in the conversion of DME to two surface methoxide (CH₃O*) species or to the methoxymethyl (CH₃OCH₂*) and hydroxyl (OH*) surface products, respectively.

The binding energies for the key intermediates involved in the initial DME combustion paths were calculated first on the ideal Pt(111) surface in the absence of oxygen; the results are summarized in Table 3. The results indicate that the DME molecule is weakly bound on Pt(111) (-19.9 kJ mol⁻¹), consistent with the reversibility assumed in the kinetic analysis described above. DME adsorption involves electron donation from the lone pair in its oxygen atom to the Pt surface. The adsorbed species lies tilted from the normal to the Pt(111) surface. As the oxygen coverages increased to 4/9 monolayer (ML) and then to 2/3 ML, the DME binding energy decreased to -12.3 and -11.0 kJ mol⁻¹, respectively. The adsorbed DME molecules at the higher coverage adopt an orientation that is nearly perpendicular to the surface to minimize repulsive interactions with neighboring chemisorbed oxygen atoms.

DME can initially react with oxygen to form either two methoxide surface intermediates or adsorbed methoxymethyl and hydroxyl intermediates. The calculated structures for these intermediates indicate that the methoxide intermediate preferentially adsorbs atop a Pt surface atom, especially as oxygen surface coverage increases. The binding energy for the methoxide intermediate on Pt(111) in the absence of coadsorbed

(40) Hinz, A.; Larsson, P. -O.; Andersson, A. *Catal. Lett.* **2002**, *78*, 177.

(41) Wu, J. C. S.; Fan, W. -C.; Lin, C. -A. *Ind. Eng. Chem. Res.* **2003**, *42*, 3225.

(42) Chantaravitoon, P.; Chavadej, S.; Schwank, J. *Chem. Eng. J.* **2004**, *97*, 161.

Table 4. DFT-Calculated Reaction Energies for the C–O and C–H Activation of Dimethyl Ether with Oxygen in the Gas Phase and over Pt(111) and Oxygen-Covered Pt(111) Surfaces

reaction	gas phase	1/9 ML O surface coverage		2/9 ML O surface coverage		4/9 ML O surface coverage		2/3 ML O surface coverage	
		E_a	ΔE_{rxn}						
$\text{DME(g)} + \text{O(g)} \rightarrow \text{CH}_3\text{OC H}_2\text{(g)} + \text{OH(g)}$	–32.8								
$\text{DME(g)} + \text{O(g)} \rightarrow 2\text{CH}_3\text{O(g)}$	–51.8								
$\text{DME}^* + \text{O}^* \rightarrow \text{CH}_3\text{OC H}_2^* + \text{OH}^*$		+114.8	–79.2 (–51.1)	+108.2	–102.0	+100.9	–104.0 (–88.4)	+99.0	–107.0 (–108.4)
$\text{DME}^* + \text{O}^* \rightarrow 2\text{CH}_3\text{O}^*$		+234.0	–7.0 (+43.9)				–9.2	+221.0	–14.0

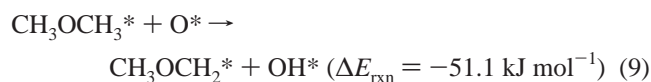
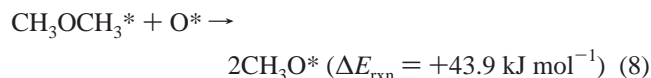
oxygen was calculated to be $-144.6 \text{ kJ mol}^{-1}$. The methoxymethyl intermediate adsorbs in a di- σ configuration via the formation of σ bonds between Pt and the CH_2 carbon and Pt and oxygen. The interaction between the surface and the CH_2 group is much stronger than with the oxygen atom. It takes on the form of a substituted methyl surface intermediate. The binding energy of the methoxymethyl intermediate on Pt(111) was calculated to be $-182.4 \text{ kJ mol}^{-1}$. The surface hydroxyl intermediate binds to atop sites with a binding energy of $-212.2 \text{ kJ mol}^{-1}$, while atomic oxygen binds at 3-fold fcc sites on the surface with a binding energy of $-365.3 \text{ kJ mol}^{-1}$.

The binding energies for all of these potential intermediates increased in the order

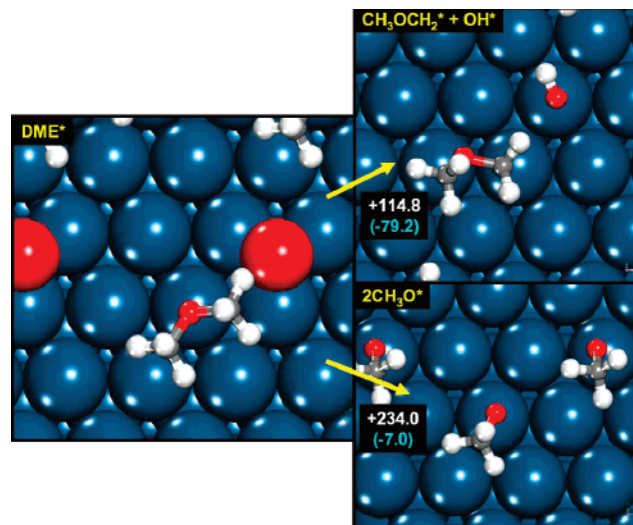


on both Pt(111) and oxygen-covered Pt(111) surfaces. The calculated binding energies are reported in Table 3 as a function of the coverage of chemisorbed oxygen. The binding energies for all these species decreased as the oxygen coverage increased. The most strongly bound intermediates showed the greatest decrease in their binding energies as oxygen coverage increased. The same binding energy rankings hold, however, at all oxygen coverages examined here.

The overall reaction energies for various proposed elementary steps were first estimated using a thermochemical cycle that neglects intermolecular interactions among adsorbed surface species:



These estimates use the adsorption energies reported in Table 3 together with the gas-phase reaction energies reported in Table 4. The C–H bond cleavage step that forms methoxymethyl intermediates ($\text{CH}_3\text{OCH}_2^*$) from molecularly adsorbed DME gives more favorable reaction energies (by 95 kJ mol^{-1}) than C–O bond cleavage to form two chemisorbed methoxide species. The reaction energy for DME to react entirely in the gas phase with a reactive atomic oxygen atom to form two methoxide radicals is 19 kJ mol^{-1} more favorable than the corresponding homogeneous reaction from DME and atomic O to form the methoxymethyl and hydroxyl radicals. This energy difference, however, is quite small and compensated in surface reactions by the larger combined heats of adsorption of $\text{CH}_3\text{OCH}_2^*$ ($-182.4 \text{ kJ mol}^{-1}$) and OH^* ($-221.2 \text{ kJ mol}^{-1}$), which are much more favorable than for two CH_3O^* species ($-289.2 \text{ kJ mol}^{-1}$ total, $-144.6 \text{ kJ mol}^{-1}$ for each methoxide species). The reactant state for both paths is the same. The selectivity

**Figure 9.** DFT-calculated structures and reaction energies for the C–H and C–O bond activation paths of DME over Pt(111) at 1/9 ML oxygen coverage.

for C–H over C–O activation, therefore, solely reflects the much greater stability of the adsorbed products formed in the C–H bond activation path. The resulting overall reaction energies from a Born-cycle analysis were calculated to be $-51.1 \text{ kJ mol}^{-1}$ for DME to form the methoxymethyl and hydroxyl surface intermediates and $+43.9 \text{ kJ mol}^{-1}$ for DME to form two methoxide intermediates (see Table 4). These calculations support the mechanistic conclusions reached on the basis of both the kinetic and isotopic analyses and described in sections 3.2 and 3.3. In contrast with CH_3OH , DME reacts via the activation of C–H bonds in molecularly adsorbed species on O^* -covered Pt surfaces.

These reactions were probed in more detail by specifically allowing reactants to form products within a given unit cell, a strategy that accounts for lateral *through-space* and *through-surface* interactions among reactant and product states. The overall reaction energies as well as the activation barriers for the two proposed DME oxidation paths were first calculated at low oxygen surface coverage, 1/9 ML. The corresponding structures for the reactant and product state are shown in Figure 9. The corresponding reaction energies are now slightly more exothermic at -79.2 and -7.0 kJ mol^{-1} for DME to form the $\text{CH}_3\text{OCH}_2^*/\text{OH}^*$ and $\text{CH}_3\text{O}^*/\text{CH}_3\text{O}^*$ surface intermediates as the result of these lateral interactions. These interactions selectively weaken reactant over product states, thus making both reactions more favorable than reported above from ideal thermodynamic cycles. The calculated activation barrier for DME reactions with chemisorbed oxygen to form methoxymethyl and OH intermediates was calculated to be $114.8 \text{ kJ mol}^{-1}$, which is much lower than the $234.0 \text{ kJ mol}^{-1}$ activation barrier

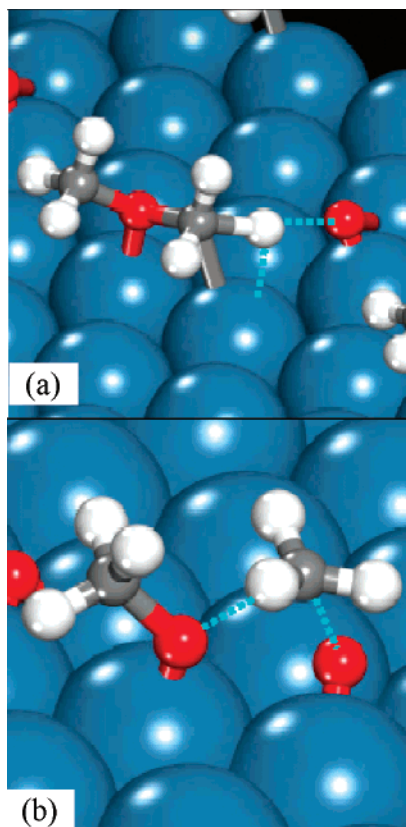


Figure 10. Isolated transition states for (a) the C–H activation of DME to form methoxymethyl and hydroxyl intermediates and (b) the C–O activation of DME to form two methoxide intermediates.

calculated for DME and chemisorbed oxygen to form two surface methoxide intermediates.

The transition-state structures isolated for both C–H bond and C–O bond activation paths to form the $\text{CH}_3\text{OCH}_2^*/\text{OH}^*$ and $\text{CH}_3\text{O}^*/\text{CH}_3\text{O}^*$ products are shown in Figure 10. The transition state for C–H activation shows the incipient stretching of the C–H bond and the interaction of the H-atom with one of the chemisorbed oxygen species. The metal atom next to that binding DME also has a bond to an oxygen atom, but it is still accessible because this oxygen resides at an fcc site on the other side of the chemisorbed DME. The availability of this neighboring Pt atom helps to stabilize both the carbon and hydrogen atoms as the C–H bond elongates and facilitates the required charge transfer. The basic oxygen atom ultimately binds with the abstracted H-atom, which acquires a more positive charge as the C–H bond is broken. The calculated barrier here is very similar to that found for the oxygen-assisted activation of methane on Pt, which is 97 kJ mol^{-1} .⁴³ The transition state to form the two methoxide species shown in Figure 10b involves the cleavage of the oxygen–methyl bond and the formation of a new oxygen–methyl bond. There is significant steric repulsion between the methyl group and the surface-bound oxygen atoms in the transition state. In addition, the metal surface does not directly participate in C–O bond activation. The CH_3 group in DME transfers directly from its oxygen to the coadsorbed oxygen without the formation of intermediate metal–carbon bonds. These two factors ultimately lead to the high activation barrier required to activate C–O bonds of DME.

(43) Janik, M. J.; Neurock, M. Unpublished results.

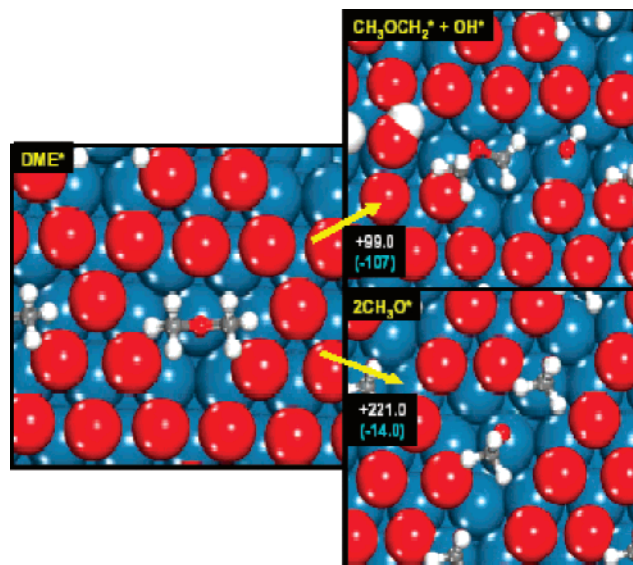


Figure 11. DFT-calculated structures and reaction energies for the C–H and C–O bond activation paths of DME over Pt(111) at 2/3 ML oxygen coverage.

These reaction paths on surfaces with low oxygen coverages may not accurately reflect the reactivity of surfaces nearly saturated with chemisorbed oxygen, which prevail during catalytic DME combustion. Thus, reaction energies were also calculated for C–O and C–H bond activation at 2/9, 4/9, and 2/3 ML of adsorbed oxygen. We present the optimized product structures for the 2/3 ML of oxygen in Figure 11 simply to illustrate the availability of sites at these higher coverages. The resulting activation and overall reaction energies studied are reported in Table 4 for each coverage. These results indicate that higher oxygen coverages lead to more favorable activation of both C–H and C–O bonds. The overall reaction energies for C–H bond activation decreased in the order -79.2 , -102.0 , -104.0 , and $-108.0 \text{ kJ mol}^{-1}$ as the oxygen coverage increased from 1/9 to 2/9, 4/9, and 2/3 ML, respectively. The activation barriers concurrently decreased in the order 114.8 (1/9 ML of O), 108.2 (2/9 ML of O), 100.9 (4/9 ML of O), and 99.0 (2/3 ML of O) kJ mol^{-1} as the oxygen coverage increased. There is a clear correlation between the activation barriers and the exothermicity of the reaction (Figure 12), as expected from ubiquitous Brønsted–Evans–Polanyi (BEP) relations. We have reported similar relationships for methane and methanol activation,⁴⁴ both of which also involve the activation of primary C–H bonds.

As the oxygen coverage increased, the transition-state structures remained effectively unchanged. The differences in coverage resulted predominantly in changes in the local electronic structure of the surface. As the oxygen surface coverage increased, the activating oxygen atom in the transition state became more weakly bound and thus more basic. This enhanced its ability to abstract hydrogen from adsorbed DME. The activation of the C–H bond of DME with oxygen can be compared with the similar step in methane reactions, because DME can be considered to be a substituted methane molecule. The transition states for the activation of DME and methane both involve stretching of a C–H bond and the formation of an O–H bond and are expected to give similar slopes in BEP

(44) Buda, C.; Neurock, M. Unpublished results.

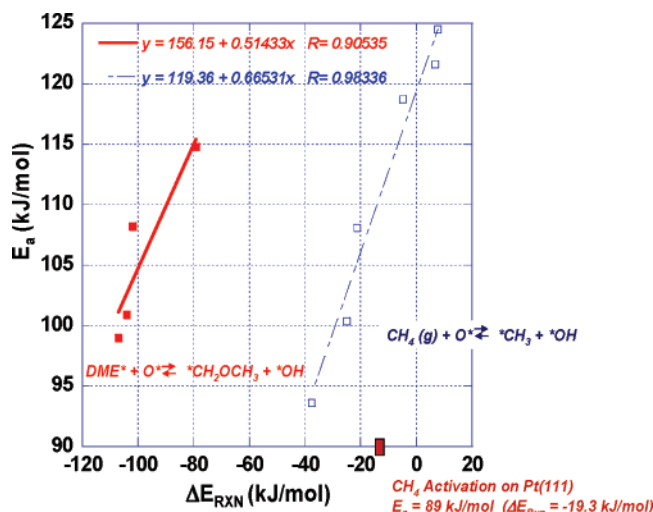


Figure 12. DFT-calculated Brønsted–Evans–Polanyi relationships for the C–H activation of DME by chemisorbed oxygen on Pt(111). The calculated BEP relationship for the C–H activation of methane by chemisorbed oxygen on Pt(111) is also shown for comparison.

relations. The two will differ, however, because the oxygen in DME ultimately interacts with the surface, thus resulting in a more exothermic reaction than for methane. There is also some interaction of the oxygen and the surface in the transition state for DME, but not in the case of methane. This would lead to slightly lower barriers and to a smaller BEP slope, consistent with the results shown in Figure 12.

The C–O activation path to form two methoxide intermediates also becomes slightly more exothermic as the coverage increased from 1/9 ML of oxygen (-7.0 kJ mol^{-1}) to 4/9 ML of oxygen (-9.2 kJ mol^{-1}) to 2/3 ML of oxygen (-14 kJ mol^{-1}). The barrier decreased from 234 to 221 kJ mol^{-1} as the oxygen coverage increased from 1/9 to 2/3 ML. We have explored only the two extremes of low and high oxygen coverages here because barriers for C–O activation were nearly twice those for the more favorable C–H activation in all cases examined.

At higher oxygen coverages, both C–H and C–O bond activation steps become more favorable. The DFT results showed that vacant sites are required to adsorb DME. This is consistent with the relevant elementary steps suggested by the kinetic and isotopic analyses described in sections 3.2 and 3.3 and with the proposed involvement of $\text{O}^*-\text{*}$ site pairs in kinetically relevant steps. As oxygen coverages increase, the C–H bond activation steps become increasingly favored over competing C–O activation steps to form methoxide species, which do not appear to be involved in DME combustion on Pt surfaces. All the theoretical results presented here indicate that reactions of DME on the oxygen-covered Pt surfaces proceed via the preferential activation of the C–H bond over the C–O bond in molecularly adsorbed DME.

The elementary-step activation energies derived from DFT can be compared with those measured from experimental DME combustion rates extrapolated to zero conversion to exclude product inhibition effects on intrinsic rates and to measure barriers corresponding to those for kinetically relevant steps. As discussed in section 3.9, measured apparent activation energies vary with Pt cluster size. Specifically, measured barriers are 104 kJ mol^{-1} on 0.8 wt % Pt/ Al_2O_3 (1.2 nm), 95 kJ mol^{-1}

on 1.0 wt % Pt/ ZrO_2 (2.7 nm), and 88 kJ mol^{-1} on 1.0 wt % Pt/ ZrO_2 (3.2 nm). The larger clusters are likely to contain greater contributions from 111 facets and resemble more closely the (111) surface used in theoretical estimates.

DFT-derived barriers can be compared with measured apparent activation energies by noting that the latter reflect the temperature dependence for the combined kinetic and thermodynamic constants in eq 6. The apparent activation energies measured reflect the activation barrier for initial C–H bond activation (E_1), the adsorption enthalpy for DME molecules ($-\Delta H_1$), and the activation barrier for O_2 dissociation (E_7) ($E_{\text{app}} = 2E_4 + 2\Delta H_1 - E_7$). DFT estimates for the C–H bond activation barrier and the enthalpy of adsorption of DME at high coverage were found to be +99 and -11 kJ mol^{-1} , respectively. The activation barrier for the activation of O_2 over a 2/3 ML of oxygen-covered Pt(111) surface was calculated from DFT to be 61 kJ mol^{-1} . The apparent activation energy calculated from these DFT-derived constants is 115 kJ mol^{-1} , in reasonable agreement with the range of experimental values reported here on supported Pt clusters ($88\text{--}104 \text{ kJ mol}^{-1}$).

3.7. Dimethyl Ether Combustion Reaction Pathways. The irreversible nature of DME and O_2 dissociation is consistent with the proposed elementary steps in Scheme 1. The proposed sequence of elementary steps (Scheme 1) for DME oxidation on Pt clusters does not involve methoxide species (step 1.2) or subsequent H-abstraction from these species (step 1.3). The catalytic sequence involves instead the kinetically relevant C–H bond activation (step 1.4) in adsorbed DME on $\text{O}^*-\text{*}$ site pairs and resembles that for CH_4 combustion on supported PdO_x clusters.¹⁸ The rate expression (eq 6) obtained from this sequence of proposed elementary steps is consistent with measured DME combustion turnover rates (Figure 3) when O^* species are the MASIs. Measured KIE values, the absence of reversible DME dissociation steps, and DFT-calculated activation barriers and reaction energies indicate that the reaction proceeds via H-abstraction from molecularly adsorbed DME in irreversible steps (step 1.4), with the C–O bond activation step occurring in subsequent steps and without any detectable kinetic relevance.

The density of oxygen vacancy sites (*) required for DME adsorption (step 1.1) depends on DME and O_2 concentrations (eq 4). Also, the concentration of these $\text{O}^*-\text{*}$ pairs depends on the quasi-equilibrated adsorption–desorption of H_2O and CO_2 as their concentrations increase with increasing DME conversion. As a result, the number of available $\text{O}^*-\text{*}$ site pairs decreases as O_2 , H_2O , and CO_2 concentrations increase and as DME concentrations decrease. Equation 6 is also consistent with the decrease in DME combustion turnover rates as a function of residence time (Figure 2), indicating that depletion of the reactant is the main reason for the observed decrease of DME combustion turnover rates with increasing residence time. The products inhibit DME combustion turnover rates by changing the concentration of $\text{O}^*-\text{*}$ pair sites; these inhibition effects are discussed in the next section.

3.8. Inhibition of Dimethyl Ether Combustion by Reaction Products. The effects of CO_2 and H_2O products on combustion rates were measured by adding CO_2 and H_2O to DME– O_2 reactant streams. These rates were measured at low DME conversions ($<1.5\%$) and a similar flow rate ($330 \text{ cm}^3 \text{ g}^{-1} \text{ s}^{-1}$). Figure 13 shows that combustion turnover rates decreased with increasing H_2O concentration, while rates were essentially

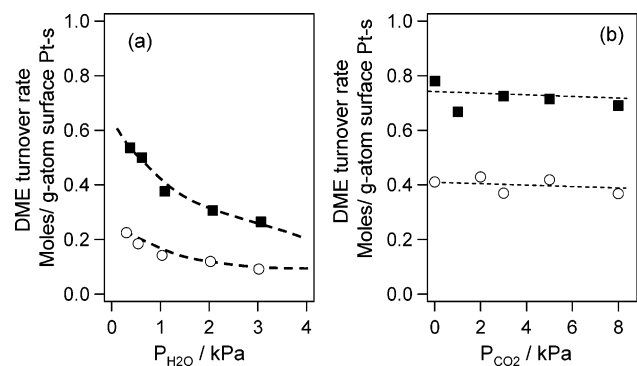


Figure 13. Effects of H₂O (a) and CO₂ (b) partial pressures on DME combustion turnover rates on 1.0 wt % Pt/ZrO₂ (5 mg, 0.42 dispersion, 250–450 μm, 50:1) at 473 K [(■) 10 kPa and (○) 50 kPa of O₂ and 2 kPa of DME].

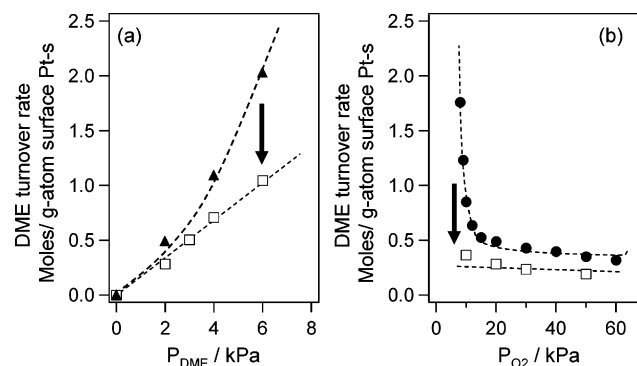


Figure 14. Effects of DME (a) and O₂ (b) partial pressures on DME combustion turnover rates with 5 kPa of H₂O (open symbols) and without H₂O (closed symbols) [1.0 wt % Pt/ZrO₂ (5 mg, 0.42 dispersion, 250–450 μm, 50:1), 473 K, 20 kPa of O₂ in (a) and 2 kPa of DME in (b)].

unaffected by CO₂ concentration. Inhibition by water reflects the reversible nature of hydroxyl recombination steps (Scheme 1, step 1.5), which leads to a decrease in the number of vacancy (*) and oxygen (O*) species, both of which are required for DME activation (Scheme 1, step 1.4). The proposed rate equation (eq 4) simplifies to the following equation when OH* species are the MASIs:

$$r = \frac{K_1 k_4 K_5 [\text{DME}]}{[\text{H}_2\text{O}]} \quad (10)$$

Turnover rates then become linear in DME pressure and independent of O₂ and decrease with increasing H₂O concentration. Figure 14 shows the effects of DME and O₂ partial pressure on combustion turnover rates in the presence of H₂O (5 kPa). For comparison, the effects of DME (20 kPa of O₂) and O₂ (2 kPa of DME) in the absence of H₂O (Figure 3) are also shown in Figure 14. Without H₂O, DME turnover rates were proportional to [DME]² and [O₂]⁻¹, consistent with eq 6 (O* = MASI). In contrast, rates increased linearly with increasing DME concentration and were almost zeroth-order in O₂ in the presence of water, consistent with the trends predicted by eq 10. The kinetic response of DME combustion rates to DME, O₂, and H₂O concentrations is similar to that for CH₄ combustion rates ([CH₄]¹, [O₂]⁰, and [H₂O]⁻¹) on supported PdO_x clusters.¹⁸ DME combustion on supported Pt clusters and CH₄ combustion on supported Pd clusters¹⁸ both involve the activation of DME and CH₄, respectively, on site pairs consisting of oxygen atoms (O*) and oxygen vacancies (*), the density of which decreases as

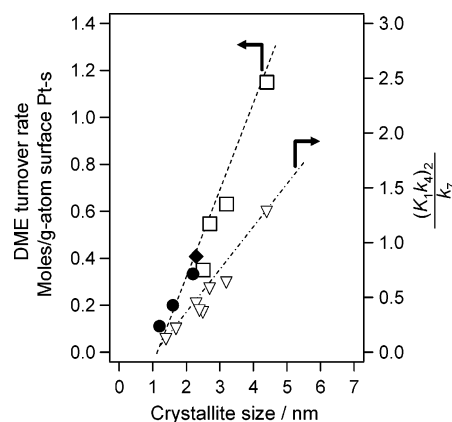


Figure 15. DME combustion turnover rates and calculated rate constants ($(K_1 k_4)^2 k_7^{-1}$) as a function of Pt cluster diameter for ZrO₂ and γ-Al₂O₃ supports [473 K, 2 kPa of DME, 20 kPa of O₂, balance He, (□) 1.0 wt % Pt/ZrO₂, (●) 1.0 wt % Pt/Al₂O₃, (◆) 2.3 wt % Pt/Al₂O₃]. Rate constants were calculated by using eq 6.

H₂O products readsorb to give significant coverages by chemisorbed OH* species.

Figure 7 also shows the parity plots for DME turnover rates calculated using the kinetic rate expression (eq 10) and measured DME turnover rates (Figure 14). It is observed that the reaction rates calculated with the kinetic expressions derived from our model are also in good agreement with measured DME turnover rates (Figure 14). The effects of DME, O₂, H₂O, and CO₂ concentrations on turnover rate are consistent with rate-determining C–H bond activation (from adsorbed DME species) on site pairs consisting of a Pt–O species and an oxygen vacancy.

The availability of vacancy sites on PdO_x surfaces during CH₄ combustion depends sensitively on oxygen and hydroxyl binding energies, which are strongly influenced, in turn, by the size of PdO_x clusters.^{15–18} The similar mechanistic requirements for these two reactions suggest that similar sensitivity to structure would be apparent in catalytic DME combustion. Such a hypothesis is examined in the next section, in which dispersion effects on DME turnover rates are reported for the first time.

3.9. Cluster Size and Support Effects on DME Combustion Turnover Rates. The effects of Pt cluster size and support (Al₂O₃, ZrO₂) on DME turnover rates are shown in Table 1 and Figure 15. DME combustion turnover rates increased with increasing Pt cluster size (Figure 15), indicating that surfaces of large Pt clusters are more effective than those of smaller clusters in catalyzing the kinetically relevant steps required for DME combustion. For a given dispersion, DME combustion turnover rates were similar on Pt/Al₂O₃ and Pt/ZrO₂ for samples with relatively high dispersions (0.26–0.99) and lower reactivity. For the most active catalysts, with the lowest dispersion (0.02–0.26), Al₂O₃ supports gave more reactive catalysts than ZrO₂ supports. As reported previously,⁴⁵ these support effects reflect bifunctional pathways in which acid sites on γ-Al₂O₃ catalyze the hydrolysis of DME to form CH₃OH using H₂O formed via DME combustion on active Pt clusters. The higher H₂O concentrations at the higher DME conversions prevalent on larger and more active Pt clusters led to stronger contributions from these bifunctional pathways and to the detection of the

(45) Ishikawa, A.; Iglesia, E. *Chem. Commun.* **2007**, 2992.

consequent bifunctional support effects on Pt catalysts with lower dispersions.

Similar effects of metal cluster size were reported for CH₄ combustion turnover rates on supported PdO_x¹⁸ and Pt clusters.⁴⁶ Smaller metal clusters exhibit a higher density of coordinately unsaturated sites, which bind oxygen more strongly than larger clusters predominantly exposing low-index surfaces.⁴⁷ Figure 15 also shows the effective rate constant, k_{effect} ($(K_1k_4)^2k_7^{-1}$), calculated using the kinetic rate expression (eq 6) and DME turnover rates measured at various residence times. The effective rate constant, k_{effect} , increased with increasing Pt cluster size. This indicates that turnover rates increase as metal clusters become larger, apparently because of a decrease in the binding energy of chemisorbed oxygen atoms increasing both the activity of O* for C–H bond activation steps (Scheme 1, step 1.4) and the availability of uncovered metal atoms (*) required for molecular chemisorption of DME (Scheme 1, step 1.1). Therefore, Pt dispersion (cluster size) strongly influences the number of O*–* site pairs available for kinetically relevant H-abstraction steps from DME adsorbates.

4. Conclusions

Isotopic measurements, kinetic dependences, and ab initio density functional theoretical calculations led to a consistent mechanistic picture of DME combustion reactions on supported Pt catalysts, involving a kinetically relevant step requiring C–H bond activation from molecular DME on a site pair consisting of an adsorbed oxygen atom and a vacancy site on Pt surfaces. Isotopic measurements as well as DFT results indicate that the initial combustion of DME proceeds via the C–H activation over O*–* site pairs to form methoxymethyl and hydroxyl surface intermediates rather than through C–O activation in

DME to produce two methoxide surface species. The absence of recombinative desorption of DME-derived intermediates and O* species was also confirmed by measurement of isotopic exchange rates. The derived rate expression from the proposed sequence of elementary steps was consistent with kinetic response of DME turnover rates to DME, O₂, H₂O, and CO₂ concentrations. The density of O*–* site pairs required for kinetically relevant H-abstraction steps from DME adsorbates was strongly affected by reactant and product concentrations and by the Pt cluster size. Theory indicates that the higher oxygen surface coverages increase the basicity of the adsorbed oxygen, thus making it more active in activating the C–H bonds of DME. Vacant sites are necessary to allow DME to bind to the surface. The observed effects of Pt crystallite size are related to changes in the density and stability of vacancies on the Pt surface and in the reactivity of surface oxygen atoms for the kinetically relevant C–H activation step.

Acknowledgment. This study was supported by BP as part of the Methane Conversion Cooperative Research Program at the University of California at Berkeley under the technical direction of Dr. Theo Fleisch. We acknowledge Drs. Aditya Bhan and Manuel Ojeda, Ms. Cathy Chin, Mr. Josef Macht, and Mr. Brian Weiss of the University of California at Berkeley for helpful technical discussions and their careful review of this manuscript. We also kindly acknowledge the computational resources provided by the Environmental Molecular Sciences Laboratory at Pacific Northwest National Laboratory.

Supporting Information Available: In situ evolution of Pt clusters during DME combustion reactions obtained from X-ray absorption spectra (Figure S1) and Appendices 1 and 2. This material is available free of charge via the Internet at <http://pubs.acs.org>.

(46) Li, M.; Chin, Y. -H.; Wei, J.; Iglesia, E. Unpublished results.

(47) Xu, Y.; Shelton, W. A.; Schneider, W. F. *J. Phys. Chem. B* **2006**, *110*, 16591.